Singular vortex dynamics on filtered Euler flows

Takeshi Gotoda
Research Institute for Electronic Science, Hokkaido University

This work is based on joint works with R. Krasny in University of Michigan and T. Sakajo in Kyoto University.

1 Introduction

1.1 Overview of the theory of turbulence

The turbulent phenomena are caused by the complex interaction of flows in the wide range of scales. This interaction in turbulent flows transfers the energy sequentially from macro scales gradually to micro scales where the energy dissipates by the viscosity. This process is known as the *energy cascade*. The theory of Kolmogorov [43] gives a mathematical description to the 3D homogeneous isotropic turbulence (cf. Frisch [28]). In his theory, it is assumed that the energy dissipation rate should converge to a finite positive value in the limit of vanishing viscosity. In other words, we can expect that solutions of the 3D Euler equations, which are formally equivalent to the zero viscous limit of the 3D Navier-Stokes equations, with the energy dissipation describe turbulent flows. However, since smooth solutions of the 3D Euler equations conserve the energy, such an anomalous energy dissipation occurs only for weak solutions.

Onsager conjectured in [56], without any rigorous proof, that weak solutions of the 3D Euler equations acquiring a Hölder continuity with the order greater than 1/3 should conserve the energy, and the energy dissipation could occur when the order is less than 1/3, which is known as *Onsager's conjecture* (cf. Eyink & Székelyhidi [25] or Shvydkoy [62]). As for the former part of the conjecture, the energy conservation, a slightly weaker statement was first proved by Eyink [22] and, then, Constantin *et al.* [13] gave a simple proof under the assumption that the solution belongs to $L^3(0,T;B^{\alpha}_{3\infty}(\mathbb{T}^3)\cap C([0,T];L^2(\mathbb{T}^3))$ with $\alpha > 1/3$, where $\mathbb{T}^3$ denotes 3D flat torus. Since the index α in the Besov space corresponds to the order of a Hölder continuity of functions, their result asserts that the energy conservation holds in the critical space of Onsager's conjecture. Subsequently, the result was proven under a slightly weaker assumption by Duchon and Robert [20] and Cheskidov *et al.* [10]. In [20], they defined *dissipative weak solutions* for the Euler equations as solutions whose energy dissipation rate is greater than or equal to zero in the sense of distribution, and then showed that the dissipation rate is zero when the Hölder continuity of weak solutions is greater than 1/3. Moreover, they showed the 4/3-law that is a statistical property in the turbulence theory predicted by Kolmogorov. Another

important statistical property, the 4/5-law, has also been shown by Eyink [24]. The latter half of Onsager's conjecture, the energy dissipation, has been studied in stages. The first example of a weak solution that breaks the energy conservation was constructed by Scheffer [59], which gives a non-trivial weak solution with a compact support in space and time $\mathbb{R}^2 \times \mathbb{R}$. A simpler construction was later shown by Shnirelman [60]. He also proved the existence of a weak solution whose energy is monotone decreasing [61]. Then, DeLellis & Székelyhidi [15, 16] extended these results to general dimension $n \geq 2$. Note that these constructed solutions are just square integrable functions in space and time, and thus not continuous in general. DeLellis and Székelyhidi have successfully constructed continuous weak solutions whose energy is not conserved [17]. Subsequently, through several contributions (cf. Buckmaster [5], Buckmaster *et al.* [6], De Lellis & Székelyhidi [16], and Isett [36, 37]), Buckmaster, DeLellis & Székelyhidi [7] have finally proven the existence of a weak solution of the 3D Euler equations that does not conserve the energy and belongs to the space $L^1(0,1;C^{1/3-\varepsilon}(\mathbb{T}^3))$ for any $\varepsilon > 0$.

As we see from the Kolmogorov-Onsager theory, non-smooth weak solutions of the 3D Euler equations with the energy dissipation may play a crucial role in understanding of 3D turbulence. However, it is uncertain what kind of fluid evolution belongs to the class of dissipative weak solutions. A motivation of this study is describing such an anomalous dissipation in terms of the physical dynamics of fluids without losing mathematical rigor. Especially, we investigate the dynamics of ideal vorticity, called *singular vortices*, such as point vortices, vortex sheets, etc., and try to make it clear what kind of vortex dynamics causes the dissipation. But, since the existence of weak solutions with singular vorticity has not been established for the 3D Euler equations, it is hard to analyze the evolution of singular vortices mathematically. To overcome this difficulty, we regularize the Euler equations in a certain manner so that their solutions with singular vorticity exist, and then take the limit of the solutions with respect to the regularization parameter. Specifically, we consider the *filtered Euler equations* that are derived by applying a spatial filter to the Euler equations. For instance, the Euler-α equations proposed by Holm, Marsden & Ratiu [32] are one of the example of the filtered Euler equations. The 3D Euler-α equations and the 3D Navier-Stokes-α equations are regarded as physically relevant models of turbulence (cf. Chen *et al.* [8, 9], Foias, Holm & Titi [26, 27] and Mohseni *et al.* [51]). In spite of its physical significance, it is still hard to tackle the 3D problem mathematically, since, for example, the existence of global solutions for the 3D Euler-α equations is as yet unknown (cf. Hou & Li [35]).

For these kinds of difficulties, we focus on the 2D turbulence flow. Many investigations (cf. Batchelor [4], Kraichnan [39] and Leith [44]) indicate that the 2D turbulence is characterized by the conservation of the energy and the dissipation of the enstrophy that is the L^2 norm of the vorticity, since there appear two inertial ranges corresponding to the backward energy cascade and the forward enstrophy cascade in the energy density spectrum at sufficiently large Reynolds number. Hence, similarly to the 3D problem, we expect that an enstrophy dissipating solution of the 2D Euler equations describes the 2D turbulent phenomena. Although the fluid dynamics in 2D flows are different from the 3D one, the 2D filtered Euler equations provide us with more theoretical advantages mathematically than the 3D ones in dealing with the present problem.

1.2 The 2D Euler equations and the enstrophy dissipation

The motion of inviscid incompressible 2D flows is described by the 2D Euler equations,

$$\partial_t \boldsymbol{u} + (\boldsymbol{u}\cdot\nabla)\boldsymbol{u} + \nabla p = 0, \qquad \operatorname{div}\boldsymbol{u} = 0, \qquad \boldsymbol{u}(\boldsymbol{x},0) = \boldsymbol{u}_0(\boldsymbol{x}), \tag{1}$$

where $\boldsymbol{u} = \boldsymbol{u}(\boldsymbol{x},t)$ is the fluid velocity field and $p = p(\boldsymbol{x},t)$ is the scalar pressure. Taking the curl of (1) and defining the vorticity field by $\omega = \operatorname{curl}\boldsymbol{u}$, we obtain the transport equation for ω,

$$\partial_t \omega + (\boldsymbol{u}\cdot\nabla)\omega = 0, \qquad \omega(\boldsymbol{x},0) = \omega_0(\boldsymbol{x}), \tag{2}$$

where $\omega_0 = \operatorname{curl}\boldsymbol{u}_0$. Then, the velocity $\boldsymbol{u}$ is recovered from the vorticity ω via the Biot-Savart law,

$$\boldsymbol{u}(\boldsymbol{x}) = (\boldsymbol{K} * \omega)(\boldsymbol{x}) = \int_{\mathbb{R}^2} \boldsymbol{K}(\boldsymbol{x}-\boldsymbol{y})\omega(\boldsymbol{y})d\boldsymbol{y}, \tag{3}$$

in which $\boldsymbol{K}$ denotes a singular integral kernel defined by

$$\boldsymbol{K}(\boldsymbol{x}) = \nabla^\perp G(\boldsymbol{x}) = -\frac{\boldsymbol{x}^\perp}{2\pi|\boldsymbol{x}|^2}, \qquad G(\boldsymbol{x}) = -\frac{1}{2\pi}\log|\boldsymbol{x}|$$

with $\nabla^\perp = (\partial_{x_2}, -\partial_{x_1})$ and $\boldsymbol{x}^\perp = (x_2, -x_1)$. Here, G is a fundamental solution to the 2D Laplacian. The Lagrangian flow map is governed by the following equation,

$$\partial_t \boldsymbol{\eta}(\boldsymbol{x},t) = \boldsymbol{u}(\boldsymbol{\eta}(\boldsymbol{x},t),t), \qquad \boldsymbol{\eta}(\boldsymbol{x},0) = \boldsymbol{x}. \tag{4}$$

Regarding the initial value problem of (2), a unique global weak solution exists for $\omega_0 \in L^1(\mathbb{R}^2)\cap L^\infty(\mathbb{R}^2)$ [49, 63]. The existence theorem can be extended to the case of $\omega_0 \in L^1(\mathbb{R}^2)\cap L^p(\mathbb{R}^2)$, $1 < p < \infty$, though the uniqueness is still open [19]. Furthermore, a global solution exists for ω_0 in the space of finite Radon measure on $\mathbb{R}^2$, denoted by $\mathcal{M}(\mathbb{R}^2)$, with a distinguished sign and its induced velocity $\boldsymbol{u}_0 \in L^2_{\mathrm{loc}}(\mathbb{R}^2)$ [18, 21, 48]. This class includes vortex sheets but not point vortices. As for the enstrophy dissipation, it has been shown in [23] that weak solutions of the 2D Euler equations with $\omega_0 \in L^p(\mathbb{R}^2)\cap L^1(\mathbb{R}^2)$, $p > 2$ can not dissipate the enstrophy in the sense of distributions. Hence, it is necessary to deal with initial vorticity in a less regular space such as $\mathcal{M}(\mathbb{R}^2)$ to obtain enstrophy dissipating solutions. But, the global solvability for the 2D Euler equations with $\omega_0 \in \mathcal{M}(\mathbb{R}^2)$ has not been established in general.

In order to construct enstrophy dissipating solutions, we consider the filtered Euler equations that are a functional generalization of the Euler-α equations and the vortex blob method [34]. The Euler-α equations and the Navier-Stokes-α equations are effective models for fluid turbulence even in 2D flows. Indeed, Lunasin *et al.* [47] numerically confirmed that the 2D Navier-Stokes-α flow acquired the inertial ranges in the energy density spectrum that correspond to the backward energy cascade and the forward enstrophy cascade for scales larger than α. On the other hand, the vortex blob method was introduced by Chorin [11] and Chorin & Bernard [12] to compute the evolution of vortex sheets [1, 41], and it has been applied to numerical simulations of incompressible flows [45]. Thus, we expect that the 2D filtered Euler equations are also a relevant model of 2D turbulent flows and effective to investigate the dynamics of the singular vorticity.

In this work, we first see the derivation of 2D filtered Euler equations and their global solvability with initial vorticity in $\mathcal{M}(\mathbb{R}^2)$ [29]. Next, we see numerical simulations of the dynamics of vortex sheets on the filtered Euler flows. This part is the joint work with Robert Krasny. Here, we use the vortex blob method for the filtering and show some vortex patterns induced by the roll-up of vortex sheets. In addition, we compare the filtered inviscid flow with a viscous flow, that is, the 2D Navier-Stokes equations from the viewpoint of the dynamics of vortex sheets. After that we focus on point vortex solutions of the 2D filtered Euler equations and show the existence of the enstrophy dissipating solutions. This part is the joint work with Takashi Sakajo. In the numerical study in [58], it is suggested that solutions of three point vortices in the Euler-α equations self-similarly collapse in the $\alpha \to 0$ limit under certain conditions and dissipate the enstrophy at the critical time. Considering the existence of self-similar collapsing solutions in the three point-vortex (PV) system [2, 38, 53], we show that there exist point vortex solutions of three filtered point-vortex system that converge to self-similar collapsing solutions of the thee PV system and dissipate the enstrophy at the time of the triple collapse.

2 The 2D filtered Euler equations

2.1 Derivation and global solvability

We derive the 2D filtered Euler equations on the basis of the framework in [26, 34]. For an incompressible velocity field $\boldsymbol{v}$, we define $\boldsymbol{u}^\varepsilon$ by

$$\boldsymbol{u}^\varepsilon(\boldsymbol{x}) = \left(h^\varepsilon * \boldsymbol{v}\right)(\boldsymbol{x}) = \int_{\mathbb{R}^2} h^\varepsilon\left(\boldsymbol{x}-\boldsymbol{y}\right)\boldsymbol{v}(\boldsymbol{y})d\boldsymbol{y}, \qquad h^\varepsilon(\boldsymbol{x}) = \frac{1}{\varepsilon^2}h\left(\frac{\boldsymbol{x}}{\varepsilon}\right) \tag{5}$$

for a radial function $h \in L^1(\mathbb{R}^2)$ satisfying $\int_{\mathbb{R}^2} h(\boldsymbol{x})d\boldsymbol{x} = 1$. We also define q and ω^ε by $q = \operatorname{curl}\boldsymbol{v}$ and $\omega^\varepsilon = \operatorname{curl}\boldsymbol{u}^\varepsilon$. Note that we have $\operatorname{div}\boldsymbol{u}^\varepsilon = 0$ and $\omega^\varepsilon = h^\varepsilon * q$ when the convolution commutes with the differential operator. We consider the Hamiltonian structure with the Hamiltonian,

$$\mathscr{E}^\varepsilon = \frac{1}{2}\int_{\mathbb{R}^2} \boldsymbol{v}(\boldsymbol{x})\cdot\boldsymbol{u}^\varepsilon(\boldsymbol{x})d\boldsymbol{x},$$

and the Lagrangian flow map $\boldsymbol{\eta}^\varepsilon$ associated with $\boldsymbol{u}^\varepsilon$:

$$\partial_t\boldsymbol{\eta}^\varepsilon(\boldsymbol{x},t) = \boldsymbol{u}^\varepsilon\left(\boldsymbol{\eta}^\varepsilon(\boldsymbol{x},t),t\right), \qquad \boldsymbol{\eta}^\varepsilon(\boldsymbol{x},0) = \boldsymbol{x}.$$

Then, the filtered Euler equations arise from an application of Hamilton's principle as follows.

$$\partial_t\boldsymbol{v} + (\boldsymbol{u}^\varepsilon\cdot\nabla)\boldsymbol{v} - (\nabla\boldsymbol{v})^T\cdot\boldsymbol{u}^\varepsilon - \nabla\Pi = 0, \qquad \operatorname{div}\boldsymbol{u}^\varepsilon = \operatorname{div}\boldsymbol{v} = 0, \tag{6}$$

where Π is a generalized pressure. Taking the curl of (6) with the incompressible condition, we obtain the transport equation for q advected by $\boldsymbol{u}^\varepsilon$:

$$\partial_t q + (\boldsymbol{u}^\varepsilon\cdot\nabla)q = 0.$$

Recalling the Biot-Savart law, $\boldsymbol{u}^\varepsilon = \boldsymbol{K} * \omega^\varepsilon$, and $\omega^\varepsilon = h^\varepsilon * q$, we obtain the vorticity form of the 2D filtered Euler equations:

$$\partial_t q + (\boldsymbol{u}^\varepsilon\cdot\nabla)q = 0, \qquad \boldsymbol{u}^\varepsilon = \boldsymbol{K}^\varepsilon * q, \qquad \boldsymbol{K}^\varepsilon = \boldsymbol{K} * h^\varepsilon. \tag{7}$$

The difference from the vorticity form of the 2D Euler equations (2) and (3) is that $\boldsymbol{K}^\varepsilon$ appears in the Biot-Savart law instead of $\boldsymbol{K}$. As shown in [29], $\boldsymbol{K}^\varepsilon$ satisfies the following properties under the assumptions of Theorem 2.1:

- $\boldsymbol{K}^\varepsilon$ is bounded in $\mathbb{R}^2$ and $\boldsymbol{K}^\varepsilon(\boldsymbol{0}) = 0$.
- $\boldsymbol{K}^\varepsilon$ vanishes at infinity with the decay rate $|\boldsymbol{x}|^{-1}$.
- $\boldsymbol{K}^\varepsilon$ is quasi-Lipschitz continuous.

These facts yield $\boldsymbol{K}^\varepsilon \in C_0(\mathbb{R}^2)$, which is the space of continuous functions vanishing at infinity, and enable us to apply a classical iterative method to construct a unique Lagrangian flow map. It is also important to remark that $\boldsymbol{K}^\varepsilon$ satisfies $\boldsymbol{K}^\varepsilon = \nabla^\perp G^\varepsilon$, where G^ε is a solution to the 2D Poisson equation, $-\Delta G^\varepsilon = h^\varepsilon$. Since h is radial, $G^\varepsilon(\boldsymbol{x}) = G^\varepsilon_r(|\boldsymbol{x}|)$ is also radial and satisfies

$$G^\varepsilon(\boldsymbol{x}) = G^1\left(\frac{\boldsymbol{x}}{\varepsilon}\right) - \frac{1}{2\pi}\log\varepsilon. \tag{8}$$

Then, we have

$$\boldsymbol{K}^\varepsilon(\boldsymbol{x}) = \frac{\boldsymbol{x}^\perp}{\varepsilon|\boldsymbol{x}|}\frac{\mathrm{d}G^1_r}{\mathrm{d}r}\left(\frac{|\boldsymbol{x}|}{\varepsilon}\right) = \boldsymbol{K}(\boldsymbol{x})P_K\left(\frac{|\boldsymbol{x}|}{\varepsilon}\right), \tag{9}$$

where $P_K(r)$ is defined by

$$P_K(r) = -2\pi r\frac{\mathrm{d}G^1_r}{\mathrm{d}r}(r). \tag{10}$$

Note that $P_K(0) = 0$ and $P_k(r) \to 1$ as $r \to \infty$. We recall that $\mathcal{M}(\mathbb{R}^2)$ denotes the space of finite Radon measures on $\mathbb{R}^2$ with the norm,

$$\|\mu\|_{\mathcal{M}} = \sup\left\{\int_{\mathbb{R}^2} f d\mu \;\middle|\; f \in C_0(\mathbb{R}^2),\ \|f\|_{L^\infty} \le 1\right\}.$$

and, for later use, define a weighting function by

$$w_{\log}(\boldsymbol{x}) = \begin{cases} (1-\log|\boldsymbol{x}|)^{-1} & ,\ |\boldsymbol{x}| \le 1, \\ 1+\log|\boldsymbol{x}| & ,\ |\boldsymbol{x}| > 1, \end{cases}$$

and, for consistency, use the notation $w_\alpha(\boldsymbol{x}) = |\boldsymbol{x}|^\alpha$ for $\boldsymbol{x} \in \mathbb{R}^2$. Then, the following theorem holds .

Theorem 2.1. [29] *Suppose that $h \in C^1_0(\mathbb{R}^2 \setminus \{0\})$ satisfies*

$$w_{\log}h,\ w_1\nabla h \in L^\infty(\mathbb{R}^2), \qquad w_1 h,\ \nabla h \in L^1(\mathbb{R}^2). \tag{11}$$

Then, for any initial vorticity $q_0 \in \mathcal{M}(\mathbb{R}^2)$, there exists a unique global weak solution of (7) such that

$$\boldsymbol{\eta}^\varepsilon \in C^1(\mathbb{R};\mathscr{G}), \quad \boldsymbol{u}^\varepsilon \in C(\mathbb{R};C(\mathbb{R}^2;\mathbb{R}^2)), \quad q \in C(\mathbb{R};\mathcal{M}(\mathbb{R}^2)),$$

where $\mathscr{G}$ denotes the group of all homeomorphism of $\mathbb{R}^2$ that preserves the Lebesgue measure.

Remark 2.2. The former condition in (11) implies that the smoothing function h may have a singularity such that

$$h(\boldsymbol{x}) \sim \mathcal{O}\left(-\log|\boldsymbol{x}|\right), \qquad \nabla h(\boldsymbol{x}) \sim \mathcal{O}\left(|\boldsymbol{x}|^{-1}\right),$$

as $|\boldsymbol{x}| \to 0$. The latter one in (11) gives the decay rate of h. All conditions in Theorem 2.1 are described in terms of the smoothing function, which allows us to apply the theorem to various filtered models including the Euler-α model and the vortex blob method.

As for the convergence of solutions of (7) to those of the 2D Euler equations, we have the following theorem.

Theorem 2.3. *Let $q_0 = \omega_0 \in L^1(\mathbb{R}^2) \cap L^\infty(\mathbb{R}^2)$. Then, for any $T > 0$, there exists $C(T) > 0$ such that*

$$\sup_{t\in[0,T]} \sup_{\boldsymbol{x}\in\mathbb{R}^2} |\boldsymbol{\eta}^\varepsilon(\boldsymbol{x},t) - \boldsymbol{\eta}(\boldsymbol{x},t)| \le C(T)\varepsilon^{e^{-T}}.$$

2.2 Euler-α model

The Euler-α model was first introduced in [32, 33] as the higher dimensional Camassa-Holm equations on the basis of the Euler-Poincaré variational framework or Lagrangian averaging to the Euler equations [50]. A remarkable property of this model is that the filtered velocity $\boldsymbol{u}^\alpha$ is written by $\boldsymbol{u}^\alpha = (1-\alpha^2\Delta)^{-1}\boldsymbol{v}$. Thus, the smoothing function h^α in (5) is defined by a fundamental solution for the operator $1-\alpha^2\Delta$, that is,

$$h^\alpha(\boldsymbol{x}) = \frac{1}{2\pi\alpha^2} K_0\left(\frac{|\boldsymbol{x}|}{\alpha}\right),$$

in which K_0 denotes the modified Bessel function of the second kind. It is important to remark that K_0 has a singularity at the origin like $K_0(r) \sim -\log r$ as $r \to 0$ and decays exponentially. Since the velocity $\boldsymbol{v}$ is explicitly expressed by the filtered velocity $\boldsymbol{u}^\alpha$, we find the following filtered Euler equations for $\boldsymbol{u}^\alpha$.

$$(1-\alpha^2\Delta)\partial_t\boldsymbol{u}^\alpha + \boldsymbol{u}^\alpha\cdot\nabla(1-\alpha^2\Delta)\boldsymbol{u}^\alpha + (\nabla\boldsymbol{u}^\alpha)^T\cdot(1-\alpha^2\Delta)\boldsymbol{u}^\alpha = \nabla\Pi,$$

which are known as the Euler-α equations. Moreover, there exist a unique global weak solution for initial vorticity $q_0 \in \mathcal{M}(\mathbb{R}^2)$, and a weak solution for $q_0 \in L^\infty(\mathbb{R}^2)\cap L^1(\mathbb{R}^2)$ converges to that of the Euler equations (2) in the $\alpha \to 0$ limit [55]. The convergence to the 2D Euler equations is extended to the case of $q_0 \in \mathcal{M}(\mathbb{R}^2)$ with a distinguished sign and $\boldsymbol{v}_0 \in L^2_{\mathrm{loc}}(\mathbb{R}^2)$ [3]. Since we have

$$\boldsymbol{K}^\alpha = \nabla^\perp G^\alpha, \qquad -\Delta G^\alpha(\boldsymbol{x}) = h^\alpha(\boldsymbol{x}),$$

G^α, $\boldsymbol{K}^\alpha$ are explicitly given by

$$G^\alpha(\boldsymbol{x}) = G^\alpha_r(|\boldsymbol{x}|) = -\frac{1}{2\pi}\left[\log|\boldsymbol{x}| + K_0\left(\frac{|\boldsymbol{x}|}{\alpha}\right)\right],$$
$$\boldsymbol{K}^\alpha(\boldsymbol{x}) = -\frac{1}{2\pi}\frac{\boldsymbol{x}^\perp}{|\boldsymbol{x}|^2} B_K\left(\frac{|\boldsymbol{x}|}{\alpha}\right) = \boldsymbol{K}(\boldsymbol{x}) B_K\left(\frac{|\boldsymbol{x}|}{\alpha}\right),$$

where $B_K(r) = 1 - rK_1(r)$ and K_1 is the first order modified Bessel function of the second kind. Note that G^α is bounded, $\boldsymbol{K}^\alpha(0) = 0$ and $B_K(r) = -2\pi r(dG_r^{\alpha=1}/dr)(r)$.

2.3 Vortex blob method

In the vortex blob method, the filtered integral kernel $\boldsymbol{K}^\sigma$ is given by

$$\boldsymbol{K}^\sigma(\boldsymbol{x}) = -\frac{1}{2\pi}\frac{\boldsymbol{x}^\perp}{|\boldsymbol{x}|^2 + \sigma^2}.$$

This regularization is also a example of the filtered Euler equations. Indeed, replacing the function h^ε in (5) by

$$h^\sigma(\boldsymbol{x}) = \frac{1}{2\pi\sigma^2}\psi\left(\frac{|\boldsymbol{x}|}{\sigma}\right), \qquad \psi(r) = \frac{2}{(r^2+1)^2},$$

we find that $\boldsymbol{K}^\sigma$ satisfies $\boldsymbol{K}^\sigma = \nabla^\perp G^\sigma$ with $-\Delta G^\sigma = h^\sigma$. Then, G^σ is expressed by

$$G^\sigma(\boldsymbol{x}) = G_r^\sigma(|\boldsymbol{x}|) = -\frac{1}{2\pi}\log\sqrt{|\boldsymbol{x}|^2 + \sigma^2},$$

and $\boldsymbol{K}^\sigma$ is rewritten by

$$\boldsymbol{K}^\sigma(\boldsymbol{x}) = \boldsymbol{K}(\boldsymbol{x})\Psi\left(\frac{|\boldsymbol{x}|}{\sigma}\right), \qquad \Psi(r) = -2\pi r\frac{dG_r^{\sigma=1}}{dr}(r) = \frac{r^2}{r^2+1}.$$

Note that both G^σ and $\boldsymbol{K}^\sigma$ are bounded on $\mathbb{R}^2$. Compared with h^α in the Euler-α model, h^σ is a bounded function and decays algebraically, that is, it is less singular and has slower decay than h^α. As for the convergence to the 2D Euler equations in the $\sigma \to 0$ limit, it has been shown in [46] that the vortex blob methods converge to weak solutions of the 2D Euler equations provided that initial vorticity belongs to $\mathcal{M}(\mathbb{R}^2)$ with a distinguished sign and its velocity field in $L^2_{\mathrm{loc}}(\mathbb{R}^2)$.

3 The motion of vortex sheets on filtered inviscid flows

3.1 Preceding result for single vortex sheet

A vortex sheet in a 2D inviscid flow can be described by a complex curve,

$$z(\Gamma, t) = x(\Gamma, t) + iy(\Gamma, t),$$

where Γ is a Lagrangian parameter describing the circulation. We consider the evolution of vortex sheets governed by the Birkhoff-Rott equation that is formally derived from the 2D Euler equations:

$$\frac{\partial}{\partial t}\overline{z}(\Gamma, t) = \frac{1}{2\pi i}\int_{-\infty}^{\infty}\frac{1}{z(\Gamma, t) - z(\widetilde{\Gamma}, t)}d\widetilde{\Gamma}, \tag{12}$$

in which $\overline{z}$ denotes complex conjugate of z and the integral in the right side is Cauchy principal value. Suppose that $p(\Gamma,t)=z(\Gamma,t)-\Gamma$ is periodic in Γ with period 1. Then, (12) is rewritten by

$$\frac{\partial}{\partial t}\overline{z}(\Gamma,t)=\frac{1}{2i}\int_0^1 \cot\pi\Big(z(\Gamma,t)-z(\widetilde{\Gamma},t)\Big)d\widetilde{\Gamma}. \tag{13}$$

We give initial data of (13) by $z(\Gamma,0)=\Gamma+p(\Gamma,0)$, where $z(\Gamma,t)=\Gamma$ is a steady solution and $p(\Gamma,0)$ is a small periodic perturbation. Due to the Kelvin-Helmholtz instability, the initial value problem of the Birkhoff-Rott equation seems to be ill-posed. Indeed, the asymptotic analysis by Moore in [52] has shown that, for the smooth initial data given by

$$z(\Gamma,0)=\Gamma+i\varepsilon\sin\Gamma,$$

a singularity forms in the vortex sheet at the critical time t_c satisfying

$$1+\frac{t_c}{2}+\ln t_c=\ln\frac{4}{\varepsilon}.$$

Moreover, Krasny gave the numerical evidence of the singularity formation in [40] with the numerical computation of vortex sheets by using the point-vortex approximation. In that study, we consider the discretization of the Birkhoff-Rott equation (13):

$$\frac{\mathrm{d}}{\mathrm{d}t}\overline{z}_j=\frac{1}{2iN}\sum_{k\neq j}^{N}\cot\pi\,(z_j-z_k), \tag{14}$$

where $z_j(t)=z(\Gamma_j,t)$ and $\Gamma_j=(j-1)/N$, $j=1,...,N$. Initial data is given by $z_j(0)=\Gamma_j+p(\Gamma_j,0)$. Note that (14) is equivalent to

$$\begin{aligned}\frac{\mathrm{d}x_j}{\mathrm{d}t}&=-\frac{1}{2N}\sum_{k\neq j}^{N}\frac{\sinh 2\pi(y_j-y_k)}{\cosh 2\pi(y_j-y_k)-\cos 2\pi(x_j-x_k)},\\ \frac{\mathrm{d}y_j}{\mathrm{d}t}&=\frac{1}{2N}\sum_{k\neq j}^{N}\frac{\sin 2\pi(x_j-x_k)}{\cosh 2\pi(y_j-y_k)-\cos 2\pi(x_j-x_k)}.\end{aligned} \tag{15}$$

To compute the dynamics of vortex sheets beyond the critical time of the singularity formation, Krasny introduced the filtered model of (15) with the vortex blob method [41].

$$\begin{aligned}\frac{\mathrm{d}x_j}{\mathrm{d}t}&=-\frac{1}{2N}\sum_{k\neq j}^{N}\frac{\sinh 2\pi(y_j-y_k)}{\cosh 2\pi(y_j-y_k)-\cos 2\pi(x_j-x_k)+\sigma^2},\\ \frac{\mathrm{d}y_j}{\mathrm{d}t}&=\frac{1}{2N}\sum_{k\neq j}^{N}\frac{\sin 2\pi(x_j-x_k)}{\cosh 2\pi(y_j-y_k)-\cos 2\pi(x_j-x_k)+\sigma^2}.\end{aligned} \tag{16}$$

We note that (16) has no singularity in the right side for $\sigma>0$ and the global solution exits. Figure 1 shows numerical solutions of (16) with initial data $z_j(0)=\Gamma_j+0.01\sin 2\pi\Gamma_j$. We see the roll-up of the vortex sheet and the solution with $\sigma=0.25$ has more turns in the core than that with $\sigma=0.5$.

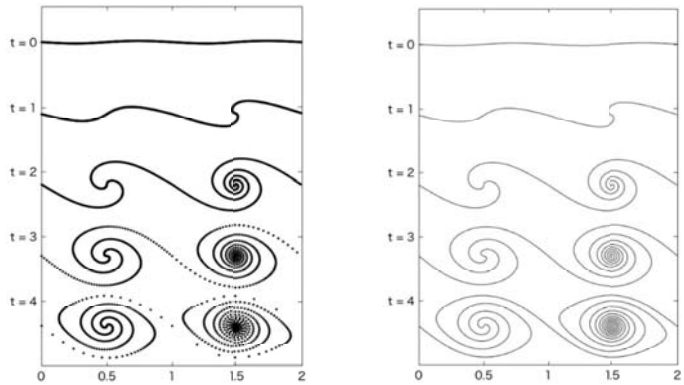

Figure 1: Numerical simulations of the single vortex sheet with the vortex blob method. The figure in the left is the plot of approximating point vortices and the right is the interpolating curve. We plot the solutions with $\sigma = 0.5$ in the interval $[0, 1]$ and $\sigma = 0.25$ in $[1, 2]$.

3.2 Numerical simulation of double vortex sheet

We see the motion of double vortex sheets on the filtered inviscid flow with the vortex blob method. The evolution of the double vortex sheet is described by the following Birkhoff-Rott equations.

$$\begin{aligned}
\frac{\partial}{\partial t}\overline{z}^{+}(\Gamma,t) &= \frac{1}{2\pi i}\int_{-\infty}^{\infty}\frac{d\widetilde{\Gamma}}{z^{+}(\Gamma,t)-z^{+}(\widetilde{\Gamma},t)} - \frac{1}{2\pi i}\int_{-\infty}^{\infty}\frac{d\widetilde{\Gamma}}{z^{+}(\Gamma,t)-z^{-}(\widetilde{\Gamma},t)},\\
\frac{\partial}{\partial t}\overline{z}^{-}(\Gamma,t) &= -\frac{1}{2\pi i}\int_{-\infty}^{\infty}\frac{d\widetilde{\Gamma}}{z^{-}(\Gamma,t)-z^{-}(\widetilde{\Gamma},t)} + \frac{1}{2\pi i}\int_{-\infty}^{\infty}\frac{d\widetilde{\Gamma}}{z^{-}(\Gamma,t)-z^{+}(\widetilde{\Gamma},t)}
\end{aligned} \tag{17}$$

with initial vortex sheets expressed by

$$z^{+}(\Gamma,0) = \Gamma + i\frac{d}{2} + p^{+}(\Gamma,0), \qquad z^{-}(\Gamma,0) = \Gamma - i\frac{d}{2} + p^{-}(\Gamma,0),$$

where z^{+} and z^{-} describe the upper vortex sheet and the lower vortex sheet respectively. The constant d denotes the distance between two vortex sheets. Under the periodic condition on Γ, the discretization of (17) is expressed by

$$\begin{aligned}
\frac{\mathrm{d}x_j^{\pm}}{\mathrm{d}t} = &-\frac{1}{2N}\sum_{k\neq j}^{N}\frac{\sinh 2\pi(y_j^{\pm}-y_k^{\pm})}{\cosh 2\pi(y_j^{\pm}-y_k^{\pm})-\cos 2\pi(x_j^{\pm}-x_k^{\pm})}\\
&+\frac{1}{2N}\sum_{k\neq j}^{N}\frac{\sinh 2\pi(y_j^{\pm}-y_k^{\mp})}{\cosh 2\pi(y_j^{\pm}-y_k^{\mp})-\cos 2\pi(x_j^{\pm}-x_k^{\mp})},
\end{aligned}$$

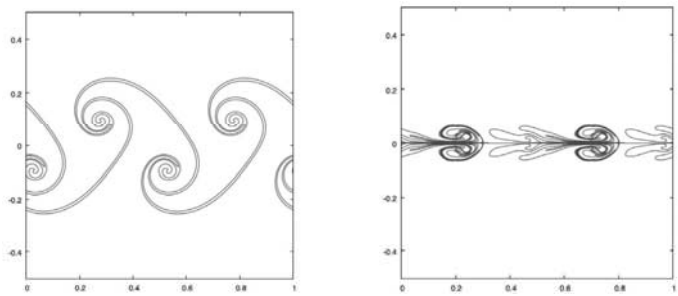

Figure 2: Numerical solutions of the filtered Birkhoff-Rott equations with $\varepsilon = 0.01$, $k = 2$, $d = 0.05$ and $\sigma = 0.15$. The left figure is a solution for the anti-symmetric mode and the right is for the symmetric one.

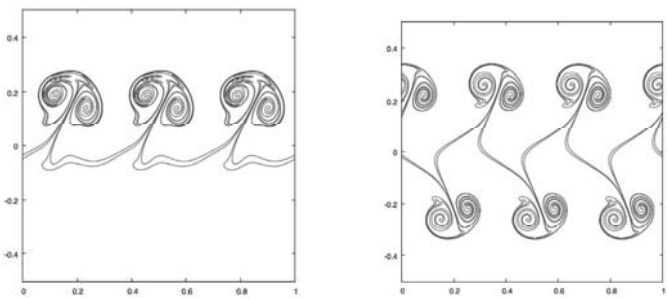

Figure 3: Numerical solutions of the filtered Birkhoff-Rott equations with a combination of the anti-symmetric and symmetric initial data ($d = 0.05$, $\sigma = 0.15$). The left figure is the anti-symmetric with $\varepsilon = 0.01$, $k = 3$ and the symmetric with $\varepsilon = 0.015$, $k = 3$. The right is the anti-symmetric with $\varepsilon = 0.06$, $k = 3$ and the symmetric with $\varepsilon = 0.02$, $k = 6$.

$$\frac{\mathrm{d}y_j^{\pm}}{\mathrm{d}t} = \frac{1}{2N}\sum_{k\neq j}^{N} \frac{\sin 2\pi(x_j^{\pm} - x_k^{\pm})}{\cosh 2\pi(y_j^{\pm} - y_k^{\pm}) - \cos 2\pi(x_j^{\pm} - x_k^{\pm})} - \frac{1}{2N}\sum_{k\neq j}^{N} \frac{\sin 2\pi(x_j^{\pm} - x_k^{\mp})}{\cosh 2\pi(y_j^{\pm} - y_k^{\mp}) - \cos 2\pi(x_j^{\pm} - x_k^{\mp})}.$$

For the numerical simulation, we use the following initial data that comes from the stability analysis for the linearized system.

$$z^{\pm}(\Gamma, 0) = \Gamma_j \pm i\frac{d}{2} + \varepsilon\left(\mp\sqrt{1 - E_k} + i\sqrt{1 + E_k}\right)\sin(2\pi k\Gamma_j), \tag{18}$$

$$z^{\pm}(\Gamma, 0) = \Gamma_j \pm i\frac{d}{2} + \varepsilon\left(\sqrt{1 + E_k} \mp i\sqrt{1 - E_k}\right)\sin(2\pi k\Gamma_j), \tag{19}$$

where $E_k = e^{-kd}$. We call (18) the anti-symmetric mode and (19) the symmetric mode. The filtered model is derived in the same manner as (16). Figure 2 shows numerical

simulations for the anti-symmetric mode and the symmetric mode. Note that initial vortex sheets are approximated by $N = 200$ point vortices and we apply the insertion of new points due to the stretching of the vortex sheets. As we see in the figures, the anti-symmetric mode produces the pattern similar to the Kármán vortex sheet and, on the other hand, the pattern of the symmetric mode is close to the jet [42]. Changing the parameters in initial data, we can observe various vortex sheet patterns, see [57]. Moreover, we consider the initial data given by linear combinations of the anti-symmetric and symmetric modes. Figure 3 shows some characteristic patterns produced by linearly combined initial data, which are observed in the real flows [14]. Note that these vortex patterns can be also produced in the single vortex sheet model [42].

3.3 Motion of vortex sheets in 2D viscous flows

We now see the motion of vortex sheets in the viscous flow governed by the 2D Navier-Stokes equations. Let $\boldsymbol{u}$ be the velocity field. We introduce the vorticity $\omega = \operatorname{curl} \boldsymbol{u}$ and the stream function ψ such that $\boldsymbol{u} = (\partial\psi/\partial y, -\partial\psi/\partial x)$. Then, the 2D Navier-Stokes equations yield

$$\frac{\partial \omega}{\partial t} + \frac{\partial \psi}{\partial y}\frac{\partial \omega}{\partial x} - \frac{\partial \psi}{\partial x}\frac{\partial \omega}{\partial y} = \nu \Delta \omega, \qquad \frac{\partial^2 \psi}{\partial x^2} + \frac{\partial^2 \psi}{\partial y^2} = -\omega, \tag{20}$$

where ν corresponds to the viscosity. Although we suppose that initial vorticity is concentrated on the 2D curve $z(\Gamma, 0) = x(\Gamma, 0) + iy(\Gamma, 0)$, we regularize it for the numerical simulation. The velocity field $\boldsymbol{u}_0(x, y) = (u_0(x, y), v_0(x, y))$ induced by the vorticity on $z(\Gamma, 0)$ is described by

$$u_0(x, y) - iv_0(x, y) = -\frac{1}{2}\int_0^1 \frac{\sinh 2\pi(y - \widetilde{y}) + i \sin 2\pi(x - \widetilde{x})}{\cosh 2\pi(y - \widetilde{y}) - \cos 2\pi(x - \widetilde{x})} d\widetilde{\Gamma}, \tag{21}$$

where $\widetilde{z} = z(\widetilde{\Gamma}, 0)$. Then, the vortex blob method gives the filtered velocity field of (21):

$$u_0^\sigma(x, y) - iv_0^\sigma(x, y) = -\frac{1}{2}\int_0^1 \frac{\sinh 2\pi(y - \widetilde{y}) + i \sin 2\pi(x - \widetilde{x})}{\cosh 2\pi(y - \widetilde{y}) - \cos 2\pi(x - \widetilde{x}) + \sigma^2} d\widetilde{\Gamma},$$

and the filtered vorticity,

$$\omega_0^\sigma(x, y) = \pi\sigma^2 \int_0^1 \frac{\cosh 2\pi(y - \widetilde{y}) + \cos 2\pi(x - \widetilde{x})}{\left(\cosh 2\pi(y - \widetilde{y}) - \cos 2\pi(x - \widetilde{x}) + \sigma^2\right)^2} d\widetilde{\Gamma}. \tag{22}$$

We use (22) as initial vorticity of (20). To see the motion of vortex sheets in (20), we consider tracer points $\boldsymbol{x}_n(0) = (x_n(0), y_n(0))$, $n = 1,...,N$ that are initially placed on the curve $z(\Gamma, 0)$ and governed by

$$\frac{\mathrm{d}}{\mathrm{d}t}\boldsymbol{x}_n(t) = \boldsymbol{u}\left(\boldsymbol{x}_n(t), t\right).$$

Figure 4 shows numerical simulations for tracers of the single vortex sheet with the same initial data in Figure 1 and the double vortex sheet with the same initial data as the right figure in Figure 3 on the Navier-Stokes flows. Their patterns of vortex sheets are similar to solutions of the filtered Birkhoff-Rott equations if both the viscosity ν and the filtering level δ are sufficiently small.

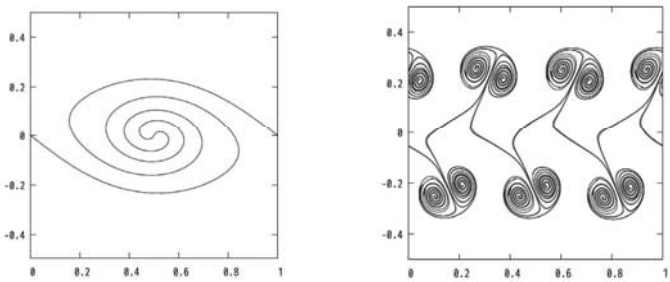

Figure 4: The left figure is tracers approximating a single vortex sheet on the Navier-Stokes flow with $z(\Gamma, 0) = \Gamma + 0.01(1 - i)\sin(2\pi\Gamma)$. The right is tracers approximating double vortex sheets on the Navier-Stokes flow with the same initial data as the right figure in Figure 3.

4 Enstrophy dissipation via triple collapse of point vortices

Suppose that the initial vorticity field is represented by a set of δ-distributions,

$$q_0(\boldsymbol{x}) = \sum_{n=1}^{N} \Gamma_n \delta(\boldsymbol{x} - \boldsymbol{x}_n^0), \tag{23}$$

where $\boldsymbol{x}_n^0 = (x_n^0, y_n^0) \in \mathbb{R}^2$ for $n = 1, \dots, N$, called *ε-point vortices*. The strength $\Gamma_n \in \mathbb{R}$ corresponds to the circulation around the ε-point vortex at $\boldsymbol{x}_n^0$. Theorem 2.1 shows that there exists a unique global weak solution to (7) with the initial data (23). More precisely, we have the following proposition.

Proposition 4.1. [31] Suppose that h satisfies the assumption of Theorem 2.1. Then, the solution to (7) with the initial data (23) is expressed by

$$q(\boldsymbol{x}, t) = \sum_{n=1}^{N} \Gamma_n \delta(\boldsymbol{x} - \boldsymbol{\eta}^\varepsilon(\boldsymbol{x}_n^0, t)). \tag{24}$$

Moreover, the point vortices on the filtered Euler flow never collapse.

The evolution of ε-point vortices is described by $\boldsymbol{x}_n^\varepsilon(t) = \boldsymbol{\eta}^\varepsilon(\boldsymbol{x}_n^0, t)$. Owing to Proposition 4.1 and (9), the equations (2.1) with the initial vorticity (23) are equivalent to

$$\frac{\mathrm{d}}{\mathrm{d}t}\boldsymbol{x}_n^\varepsilon(t) = \boldsymbol{u}^\varepsilon(\boldsymbol{x}_n^\varepsilon(t), t) = -\frac{1}{2\pi}\sum_{m\neq n}^{N} \Gamma_m \frac{(\boldsymbol{x}_n^\varepsilon - \boldsymbol{x}_m^\varepsilon)^\perp}{(l_{mn}^\varepsilon)^2} P_K\left(\frac{l_{mn}^\varepsilon}{\varepsilon}\right), \tag{25}$$

for $n = 1, \dots, N$, where $l_{mn}^\varepsilon(t) = |\boldsymbol{x}_n^\varepsilon(t) - \boldsymbol{x}_m^\varepsilon(t)|$ and $\boldsymbol{x}_n^\varepsilon(0) = \boldsymbol{x}_n^0$. We call the system (25) the *filtered point-vortex (FPV) system*. According to Proposition 4.1, a weak solution to the 2D filtered Euler equations provides a solution of the FPV system and vice versa. Let us see some properties of the FPV system. Considering the relation

$$G_r^\varepsilon(|\boldsymbol{x}|) = -\frac{1}{2\pi}\left[\log|\boldsymbol{x}| + H_G\left(\frac{|\boldsymbol{x}|}{\varepsilon}\right)\right], \qquad H_G(r) = -\log r - 2\pi G_r^1(r), \tag{26}$$

we find that (25) is a Hamiltonian dynamical system, that is,

$$\Gamma_n \frac{\mathrm{d}x_n^\varepsilon}{\mathrm{d}t} = \frac{\partial \mathscr{H}^\varepsilon}{\partial y_n^\varepsilon}, \qquad \Gamma_n \frac{\mathrm{d}y_n^\varepsilon}{\mathrm{d}t} = -\frac{\partial \mathscr{H}^\varepsilon}{\partial x_n^\varepsilon},$$

with the Hamiltonian,

$$\mathscr{H}^\varepsilon = -\frac{1}{2\pi}\sum_{n=1}^{N}\sum_{m=n+1}^{N}\Gamma_n\Gamma_m\left[\log l_{mn}^\varepsilon + H_G\left(\frac{l_{mn}^\varepsilon}{\varepsilon}\right)\right]. \tag{27}$$

The FPV system (25) for $N \leq 3$ is integrable for any strengths of point vortices. It is also integrable for $N = 4$ when the total vortex strength is zero, i.e. $\Gamma \equiv \sum_{n=1}^{N}\Gamma_n = 0$. In the case $N = 4$ with $\Gamma \neq 0$ or $N \geq 5$, the system is no longer integrable and the dynamics of ε-point vortices could be chaotic. Let us introduce an important conserved quantity M^ε defined by

$$M^\varepsilon = \sum_{n\neq m}^{N}\Gamma_n\Gamma_m(l_{mn}^\varepsilon)^2 = 2(\Gamma I^\varepsilon - (Q^\varepsilon)^2 - (P^\varepsilon)^2),$$

which depends only on the distances l_{mn}^ε.

4.1 Variations of energy and enstrophy

We are concerned with the enstrophy and the energy varying with the evolution of ε-point vortices, which are derived on the basis of the Novikov's method [54, 58]. We define the Fourier transform of $f(\boldsymbol{x})$ and the Hankel transform of $f_r(|\boldsymbol{x}|) = f(\boldsymbol{x})$ by

$$\mathscr{F}[f](\boldsymbol{k}) = \frac{1}{2\pi}\int_{\mathbb{R}^2} f(\boldsymbol{x})e^{-i\boldsymbol{x}\cdot\boldsymbol{k}}d\boldsymbol{x}, \qquad \widehat{f}(s) = \mathscr{F}[f](\boldsymbol{k}) = \int_0^\infty r f_r(r)J_0(rs)dr$$

respectively, in which $r = |\boldsymbol{x}|$ and $s = |\boldsymbol{k}|$. The total enstrophy for the filtered vorticity is given by

$$\frac{1}{2}\int_{\mathbb{R}^2}|\omega^\varepsilon(\boldsymbol{x},t)|^2\,d\boldsymbol{x} = \frac{1}{2}\int_{\mathbb{R}^2}|\mathscr{F}[\omega^\varepsilon](\boldsymbol{k},t)|^2\,d\boldsymbol{k} = \int_0^\infty \pi s\langle|\mathscr{F}[\omega^\varepsilon](s,t)|^2\rangle ds,$$

where $\langle f\rangle = \frac{1}{2\pi}\int_{-\pi}^{\pi} f(\theta)d\theta$ and we define the enstrophy density spectrum $\mathscr{Z}_N^\varepsilon(s,t) = \pi s\langle|\mathscr{F}[\omega^\varepsilon](s,t)|^2\rangle$. The Fourier transform of the vorticity (24) is represented by

$$\mathscr{F}[q](\boldsymbol{k},t) = \frac{1}{2\pi}\sum_{n=1}^{N}\Gamma_n e^{-i\boldsymbol{k}\cdot\boldsymbol{x}_n^\varepsilon(t)}.$$

Hence, we have

$$|\mathscr{F}[q](\boldsymbol{k},t)|^2 = \frac{1}{4\pi^2}\left[\sum_{n=1}^{N}\Gamma_n^2 + 2\sum_{n=1}^{N}\sum_{m=n+1}^{N}\Gamma_n\Gamma_m\cos\left(\boldsymbol{k}\cdot(\boldsymbol{x}_n^\varepsilon(t) - \boldsymbol{x}_m^\varepsilon(t))\right)\right].$$

Since h^ε is radial and $\omega^\varepsilon = h^\varepsilon * q$ yields $\mathscr{F}[\omega^\varepsilon] = 2\pi\mathscr{F}[h^\varepsilon]\mathscr{F}[q]$, we obtain

$$\begin{aligned}\mathscr{Z}_N^\varepsilon(s,t) &= \frac{s}{4\pi}\left|2\pi\widehat{h^\varepsilon}(s)\right|^2\left[\sum_{n=1}^N\Gamma_n^2 + 2\sum_{n=1}^N\sum_{m=n+1}^N\Gamma_n\Gamma_m\frac{1}{2\pi}\int_{-\pi}^{\pi}\cos\left(sl_{mn}^\varepsilon\cos\theta\right)d\theta\right]\\ &= \frac{s}{4\pi}\left|2\pi\widehat{h^\varepsilon}(s)\right|^2\left[\sum_{n=1}^N\Gamma_n^2 + 2\sum_{n=1}^N\sum_{m=n+1}^N\Gamma_n\Gamma_m J_0\left(sl_{mn}^\varepsilon\right)\right],\end{aligned}$$

where $J_0(s)$ is a Bessel function of the first kind. Thus, the total enstrophy for the FPV system is expressed by

$$\begin{aligned}&\frac{1}{2}\int_{\mathbb{R}^2}\left|\omega^\varepsilon(\boldsymbol{x},t)\right|^2 d\boldsymbol{x} = \int_0^\infty \mathscr{Z}_N^\varepsilon(s,t)ds\\ &= \frac{1}{4\pi\varepsilon^2}\sum_{n=1}^N\Gamma_n^2\int_0^\infty s\left|2\pi\widehat{h}(s)\right|^2 ds + \frac{1}{2\pi\varepsilon^2}\sum_{n=1}^N\sum_{m=n+1}^N\Gamma_n\Gamma_m\int_0^\infty s\left|2\pi\widehat{h}(s)\right|^2 J_0\left(s\frac{l_{mn}^\varepsilon}{\varepsilon}\right)ds.\end{aligned}$$

Here, we use the relation $\widehat{h^\varepsilon}(s) = \widehat{h}(\varepsilon s)$. Since the first term in the right side is constant in time, the variational part of the enstrophy is given by

$$\mathscr{Z}^\varepsilon(t) \equiv \frac{1}{2\pi\varepsilon^2}\sum_{n=1}^N\sum_{m=n+1}^N\Gamma_n\Gamma_m\int_0^\infty s\left|2\pi\widehat{h}(s)\right|^2 J_0\left(s\frac{l_{mn}^\varepsilon(t)}{\varepsilon}\right)ds. \tag{28}$$

The total energy for the filtered velocity is defined by

$$\frac{1}{2}\int_{\mathbb{R}^2}\left|\boldsymbol{u}^\varepsilon(\boldsymbol{x},t)\right|^2 d\boldsymbol{x} = \int_0^\infty \pi s\langle\left|\mathscr{F}[\boldsymbol{u}^\varepsilon](s,t)\right|^2\rangle ds.$$

Since $\left|\mathscr{F}[\omega^\varepsilon](\boldsymbol{k},t)\right|^2 = |\boldsymbol{k}|^2\left|\mathscr{F}[\boldsymbol{u}^\varepsilon](\boldsymbol{k},t)\right|^2$, the energy density spectrum E_N^ε is expressed by

$$E_N^\varepsilon(s,t) \equiv \pi s\langle\left|\mathscr{F}[\boldsymbol{u}^\varepsilon](s,t)\right|^2\rangle = \frac{1}{4\pi s}\left|2\pi\widehat{h^\varepsilon}(s)\right|^2\left[\sum_{n=1}^N\Gamma_n^2 + 2\sum_{n=1}^N\sum_{m=n+1}^N\Gamma_n\Gamma_m J_0\left(sl_{mn}^\varepsilon\right)\right].$$

Hence, the total energy cut off at a scale larger than $1 \ll L < \infty$ is expressed by

$$\begin{aligned}\int_{L^{-1}}^\infty E_N^\varepsilon(s,t)dr &= \frac{1}{4\pi}\sum_{n=1}^N\Gamma_n^2\int_{\varepsilon L^{-1}}^\infty\frac{1}{s}\left|2\pi\widehat{h}(s)\right|^2 ds\\ &\quad + \frac{1}{2\pi}\sum_{n=1}^N\sum_{m=n+1}^N\Gamma_n\Gamma_m\int_{\varepsilon L^{-1}}^\infty\frac{1}{s}\left|2\pi\widehat{h}(s)\right|^2 J_0\left(s\frac{l_{mn}^\varepsilon}{\varepsilon}\right)ds.\end{aligned} \tag{29}$$

The second term is rewritten by

$$\begin{aligned}&\int_{\varepsilon L^{-1}}^\infty\frac{1}{s}\left|2\pi\widehat{h}(s)\right|^2 J_0\left(s\frac{l_{mn}^\varepsilon}{\varepsilon}\right)ds\\ &= \int_{\varepsilon L^{-1}}^\infty\frac{1}{s}J_0\left(s\frac{l_{mn}^\varepsilon}{\varepsilon}\right)ds + \int_{\varepsilon L^{-1}}^\infty\frac{1}{s}\left(\left|2\pi\widehat{h}(s)\right|^2 - 1\right)J_0\left(s\frac{l_{mn}^\varepsilon}{\varepsilon}\right)ds,\end{aligned}$$

and the following approximation holds for a sufficiently large L.

$$\int_{\varepsilon L^{-1}}^{\infty} \frac{1}{s} J_0\left(s\frac{l_{mn}^{\varepsilon}}{\varepsilon}\right) ds \sim -\log l_{mn}^{\varepsilon} + \log\frac{Le^{\beta}}{2} + \mathcal{O}\left(L^{-2}\log L^{-1}\right),$$

in which β is the Euler's constant. Taking the $L\to\infty$ limit in the non-constant part of the total energy (29), we obtain the variational part of the energy:

$$E^{\varepsilon}(t) \equiv -\frac{1}{2\pi}\sum_{n=1}^{N}\sum_{m=n+1}^{N}\Gamma_n\Gamma_m\left[\log l_{mn}^{\varepsilon}(t) + \int_0^{\infty}\frac{1}{s}\left(1-\left|2\pi\widehat{h}(s)\right|^2\right)J_0\left(s\frac{l_{mn}^{\varepsilon}(t)}{\varepsilon}\right)ds\right]. \tag{30}$$

Note that the integrand of the second term has no singularity, owing to $2\pi\widehat{h}(0)=1$.

4.2 The three ε-vortex problem and the enstrophy dissipation

We consider the three ε-point vortex problem, i.e. the FPV system with $N=3$. In order to take the $\varepsilon\to 0$ limit, we introduce the following scaled variables:

$$\boldsymbol{X}_n(t) = \frac{1}{\varepsilon}\boldsymbol{x}_n^{\varepsilon}(\varepsilon^2 t + t^*), \qquad L_{mn}(t) = \frac{1}{\varepsilon}l_{mn}^{\varepsilon}(\varepsilon^2 t + t^*) \tag{31}$$

for $m,n=\{1,2,3\}$ with $m\neq n$, where $t^*\in\mathbb{R}$ is an arbitrary constant determined later. Then, the evolution equation for $\boldsymbol{X}_n(t)$ is described by

$$\frac{\mathrm{d}}{\mathrm{d}t}\boldsymbol{X}_n = -\frac{1}{2\pi}\sum_{m\neq n}^{3}\Gamma_m\frac{(\boldsymbol{X}_n-\boldsymbol{X}_m)^{\perp}}{L_{mn}^2}P_K\left(L_{mn}\right), \qquad \boldsymbol{X}_n(0) = \frac{\boldsymbol{x}_n^{\varepsilon}(t^*)}{\varepsilon}. \tag{32}$$

This is a Hamiltonian system with the Hamiltonian,

$$\mathscr{H} = -\frac{1}{2\pi}\left[\Gamma_2\Gamma_3 H_P\left(L_{23}^2\right) + \Gamma_3\Gamma_1 H_P\left(L_{31}^2\right) + \Gamma_1\Gamma_2 H_P\left(L_{12}^2\right)\right], \tag{33}$$

where $H_P(r) = \log\sqrt{r} + H_G\left(\sqrt{r}\right)$, and the invariant quantity,

$$M = \Gamma_2\Gamma_3 L_{23}^2 + \Gamma_3\Gamma_1 L_{31}^2 + \Gamma_1\Gamma_2 L_{12}^2. \tag{34}$$

The relative equilibria of (32) are equilateral triangles or collinear configurations, see Proposition 1 of [30] for its proof. In terms of the scaled variables, the variation of the enstrophy $\mathscr{Z}^{\varepsilon}(t)$ is rewritten by

$$\mathscr{Z}^{\varepsilon}(t) = -\frac{1}{\varepsilon^2}\mathscr{Z}_0\left(\frac{t-t^*}{\varepsilon^2}\right), \qquad \mathscr{Z}_0(\tau) = -\frac{1}{2\pi}\sum_{n=1}^{N}\sum_{m=n+1}^{N}\Gamma_n\Gamma_m Z_{mn}(\tau), \tag{35}$$

$$Z_{mn}(\tau) = \int_0^{\infty} s\left|2\pi\widehat{h}(s)\right|^2 J_0\left(sL_{mn}(\tau)\right)ds. \tag{36}$$

As for the variation of the energy $E^{\varepsilon}(t)$, we rewrite (30) as

$$E^{\varepsilon}(t) = \mathscr{H}^{\varepsilon} + E_0\left(\frac{t-t^*}{\varepsilon^2}\right), \qquad E_0(\tau) = -\frac{1}{2\pi}\sum_{n=1}^{N}\sum_{m=n+1}^{N}\Gamma_n\Gamma_m E_{mn}(\tau),$$

$$E_{mn}(\tau) = -H_G\left(L_{mn}(\tau)\right) + \int_0^\infty \frac{1}{s}\left(1 - \left|2\pi\widehat{h}(s)\right|^2\right) J_0\left(sL_{mn}(\tau)\right) ds.$$

The energy dissipation rate $\mathscr{D}_E^\varepsilon$ is defined by differentiating $E^\varepsilon(t)$:

$$\mathscr{D}_E^\varepsilon(t) = \frac{1}{\varepsilon^2}\frac{\mathrm{d}E_0}{\mathrm{d}\tau}\left(\frac{t-t^*}{\varepsilon^2}\right).$$

Before stating main theorems, let us mention the connection with the self-similar collapse of three point vortices in the PV system. The PV system admits two invariants: one is the Hamiltonian $\mathscr{H}_{\rm pv} = -\frac{1}{2\pi}(\Gamma_2\Gamma_3\log l_{23} + \Gamma_3\Gamma_1\log l_{31} + \Gamma_1\Gamma_2\log l_{12})$ and the other is $M_{\rm pv} = \Gamma_2\Gamma_3 l_{23}^2 + \Gamma_3\Gamma_1 l_{31}^2 + \Gamma_1\Gamma_2 l_{12}^2$ where l_{ij} denotes the distance between two point vortices. It is well-known that the condition

$$\frac{1}{\Gamma_1} + \frac{1}{\Gamma_2} + \frac{1}{\Gamma_3} = 0, \tag{37}$$

and $M_{\rm pv} = 0$ are the necessary and sufficient conditions for three point vortices to collapse self-similarly in a finite time [2, 38]. On the other hand, for arbitrary solutions of the FPV system (32), it follows from (31) that $M^\varepsilon = \varepsilon^2 M \to 0$ as $\varepsilon \to 0$. Hence, whatever value of M^ε we choose, the condition of the existence of the triple collapse of point vortices is automatically satisfied in the limit of $\varepsilon \to 0$.

To state the theorem, we assume $\Gamma_1 \geq \Gamma_2 > 0 > \Gamma_3$ without loss of generality and remark that (37) yields $\mathscr{H}^\varepsilon = \mathscr{H}$. We also introduce the following function and constants defined only from the strengths Γ_1 and Γ_2,

$$\psi(r) = \left(\frac{1}{1+r}\right)^{1/\Gamma_1}\left(\frac{r}{1+r}\right)^{1/\Gamma_2}, \quad k_\pm = \left(\frac{\Gamma_1+\Gamma_2 \pm \sqrt{\Gamma_1^2+\Gamma_1\Gamma_2+\Gamma_2^2}}{\Gamma_2}\right)^2, \tag{38}$$

and k_0 is either k_- or k_+ such that

$$k_0 = \operatorname*{argmin}_{k\in\{k_+,k_-\}} \psi\left(\frac{\Gamma_1}{\Gamma_2}k\right).$$

Theorem 4.2. [31] Let $h \in C^1(\mathbb{R}^2)$ be a positive radial function satisfying (11), $\int_{\mathbb{R}^2} h = 1$, $w_{3+\eta}h \in L^\infty(\mathbb{R}^2)$ with $\eta > 0$, $w_1\nabla h \in L^1(\mathbb{R}^2)$ and $h_r' < 0$. Suppose (37) and the constant $\mathscr{H}_c$ satisfies

$$\frac{\Gamma_1^2\Gamma_2^2}{4\pi(\Gamma_1+\Gamma_2)}\log\left(\psi\left(\frac{\Gamma_1}{\Gamma_2}k_0\right)\left[\psi\left(\frac{\Gamma_1}{\Gamma_2}\right)\right]^{-1}\right) < \mathscr{H}_c < 0. \tag{39}$$

We also assume that, for any initial configuration with $\mathscr{H}^\varepsilon = \mathscr{H}_c$, the corresponding solution of (32) does not converge to a relative equilibrium as either of $t \to \pm\infty$. Then, there exists a constant t^* such that $l_{mn}^\varepsilon(t^*) \to 0$ as $\varepsilon \to 0$ and

$$\lim_{\varepsilon\to 0}\mathscr{Z}^\varepsilon = -z_0\delta(\cdot - t^*), \qquad \lim_{\varepsilon\to 0}\mathscr{D}_E^\varepsilon = 0$$

in the sense of distributions, where $z_0 = \int_{-\infty}^\infty \mathscr{Z}_0(\tau)d\tau$.

Theorem 4.2 asserts that the enstrophy variation converges to the δ-measure with the mass of $-z_0$ as $\varepsilon \to 0$. However, it is still unknown whether the enstrophy always dissipates in that limit, since the sign of z_0 has not yet been determined. The following corollary gives a sufficient condition for the enstrophy dissipation, which is described in terms of the function $Z(r)$ defined by

$$Z(r) = \int_0^\infty s \left|2\pi\widehat{h}(s)\right|^2 J_0\left(s\sqrt{r}\right) ds. \tag{40}$$

Corollary 4.3. [31] Suppose that $Z(r)$ is monotone decreasing and concave. Then, for any initial configuration satisfying the assumptions of Theorem 4.2 and $M \geq 0$, we have $z_0 > 0$. For the case of $M < 0$, we have $z_0 > 0$ provided that $Z(r)$ and $H_P(r)$ satisfy the additional condition,

$$Z''(r)H_P'(r) - Z'(r)H_P''(r) > 0. \tag{41}$$

Regarding the $\varepsilon \to 0$ limit of solutions obtained in Theorem 4.2, they converge to the self-similar collapsing and expanding solutions in the three PV system.

Theorem 4.4. [31] Under the same assumptions of Theorem 4.2, in the $\varepsilon \to 0$ limit, the solution of (25) with $N = 3$ converges to the self-similar collapsing solution for $t < t^*$ and the expanding solution for $t > t^*$ with the same value of the Hamiltonian $\mathscr{H}_{\rm pv} = \mathscr{H}_c$ in the three PV system.

This indicates that the three ε-point vortices collapse self-similarly at $t = t^*$ in the $\varepsilon \to 0$ limit. Hence the enstrophy dissipation occurs at the event of the collapse. Since $M^{\varepsilon\to 0} = 0$ is automatically satisfied, only (37) becomes the essential condition for the self-similar collapse. In addition, the condition (39) is required, since, in the three PV system, the Hamiltonian $\mathscr{H}_{\rm pv}$ should also be in the same range of (39) for the existence of the self-similar collapse, see Lemma 1 in [30]. We remark that the divergence of $L_{mn}(t)$ plays an essential role in the proofs of Theorem 4.2, 4.4, and that (37) is the necessary condition for the existence of the enstrophy dissipation via the triple collapse.

Theorem 4.5. [31] Suppose $L_{mn}(t) \to +\infty$ as $t \to \pm\infty$ for $m \neq n$. Then, (37) holds.

References

[1] Anderson, C.: A vortex method for flows with slight density variations. J. Comput. Phys. **61**, 417-444 (1985)

[2] Aref, H.: Motion of three vortices. Phys. Fluids, **22**(3), 393-400 (1979)

[3] Bardos, C., Linshiz, J. S. and Titi, E. S.: Global regularity and convergence of a Birkhoff-Rott-α approximation of the dynamics of vortex sheets of the two-dimensional Euler equations. Commun. Pure Appl. Maths **63** 2010, 697-746.

[4] Batchelor, G. K.: Computation of the energy spectrum in homogeneous two-dimensional turbulence. Phys. Fluids Suppl. II, **12**, 233-239 (1969)

[5] Buckmaster, T.: Onsager's conjecture almost everywhere in time. Comm. Math. Phys. 333, 1175-1198 (2015)

[6] Buckmaster, T., De Lellis, C., Isett, P. and Székelyhidi, L., Jr: Anomalous dissipation for 1/5-Hölder Euler flows. Ann. of Math. **181**, 127-172 (2015)

[7] Buckmaster, T., De Lellis, C. and Székelyhidi, L. Jr: Dissipative Euler flows with Onsager-critical spacial regularity. Comm. Pure Appl. Math., **69**, 1613-1670 (2016)

[8] Chen, S., Foias, C., Holm, D. D., Olson, E., Titi, E. S. and Wynne, S.: Camassa-Holm equations as a closure model for turbulent channel and pipe flow. Phy. Rev. Lett. **81**(24), 5338-5341 (1998)

[9] Chen, S., Holm, D. D., Margolin, L. G. and Zhang, R.: Direct numerical simulations of the Navier-Stokes alpha model. Physica D **133**, 66-83 (1999)

[10] Cheskidov, A., Constantin, P., Friedlander, S., and Shvydkoy, R.: Energy conservation and Onsager's conjecture for the Euler equations. Nonlinearity **21**, 1233-1252 (2008).

[11] Chorin, A. J.: Numerical study of slightly viscous flow. J. Fluid Mech. **57**, 785-796 (1973)

[12] Chorin, A. J. and Bernard, P. S.: Discretization of a vortex sheet, with an example of roll-up. J. Comput. Phys. **13**, 423-429 (1973)

[13] Constantin, P., E, W., and Titi, E. S.: Onsager's Conjecture on the Energy Conservation for Solutions of Euler's Equation. Comm. Math. Phys. **165**, 207-209 (1994)

[14] Couder, Y. and Basdevant, C.: Experimental and numerical study of vortex couples in two-dimensional flows. J. Fluid Mech., **173**, 225-251 (1986)

[15] De Lellis, C. and Székelyhidi, L. Jr: The Euler equations as a differential inclusion. Ann. of Math. **170**, 1417-1436 (2009)

[16] De Lellis, C. and Székelyhidi, L. Jr: On admissibility criteria for weak solutions of the Euler equations. Arch. Ration. Mech. Anal. **195** 225-260 (2010)

[17] De Lellis, C. and Székelyhidi, L. Jr: Dissipative continuous Euler flows. Invent. Math. **193**, 377-407 (2013)

[18] Delort, J.-M.: Existence de nappe de tourbillion en dimension deux. J. Amer. Math. Soc., **4**, 553-586 (1991)

[19] Diperna, R. J. and Majda, A. J.: Concentrations in regularizations for 2-D incompressible flow. Comm. Pure Appl. Math., **40**, 301-345 (1987)

[20] Duchon, J. and Robert, R.: Inertial energy dissipation for weak solutions of incompressible Euler and Navier-Stokes equations. Nonlinearity **13**, 249-255 (2000)

[21] Evans, L. C. and Müller, S.: Hardy spaces and the two-dimensional Euler equations with nonnegative vorticity. J. Amer. Math. Soc. **7**, 199-218 (1994)

[22] Eyink, G. L.: Energy dissipation without viscosity in ideal hydrodynamics. I. Fourier analysis and local energy transfer. Physica D **78**, 222-240 (1994)

[23] Eyink, G. L.: Dissipation in turbulent solutions of 2D Euler equations. Nonlinearity, **14**, 787-802 (2001)

[24] Eyink, G. L.: Local 4/5-law and energy dissipation anomaly in turbulence. Nonlinearity **21**, 1233-1252 (2003).

[25] Eyink, G. L. and Sreenivasan, K. R.: Onsager and the theory of hydrodynamic turbulence. Rev. Mod. Phys. **78**, 87-135 (2006).

[26] Foias, C., Holm, D. D. and Titi, E. S.: The Navier-Stokes-alpha model of fluid turbulence. Physica D **152-153**, 505-519 (2001)

[27] Foias, C., Holm, D. D. and Titi, E. S.: The three dimensional viscous Camassa-Holm equations, and their relation to the Navier-Stokes equations and turbulence theory. J. Dyn. Diff. Equ. **14**, 1-35 (2002)

[28] Frisch, U.: Turbulence. Cambridge University Press, Cambridge, (1995)

[29] Gotoda, T.: Global solvability for two-dimensional filtered Euler equations with measure valued initial vorticity. Differential Integral Equations, **31**, no.11-12, 851-870 (2018)

[30] Gotoda, T. and Sakajo, T.: Distributional enstrophy dissipation via the collapse of triple point vortices. J. Nonlinear Sci., **26**, 1525-1570 (2016)

[31] Gotoda, T. and Sakajo, T.: Universality of the anomalous enstrophy dissipation at the collapse of three point vortices on Euler-Poincaré models. SIAM J. Appl. Math., **78**, 2105-2128 (2018)

[32] Holm, D. D., Marsden, J. E. and Ratiu, T. S.: Euler-Poincaré models of ideal fluids with nonlinear dispersion. Phys. Rev. Lett., **80**, 4173-4177 (1998)

[33] Holm, D. D., Marsden, J. E. and Ratiu, T. S.: Euler-Poincaré equations and semidirect products with applications to continuum theories. Adv. Maths., **137**, 1-81 (1998)

[34] Holm, D. D., Nitsche, M. and Putkaradze, V.: Euler-alpha and vortex blob regularization of vortex filament and vortex sheet motion. J. Fluid Mech. **555**, 149-176 (2006)

[35] Hou, T. Y. and Li, C.:On global well-posedness of the Lagrangian averaged Euler equations. SIAM J. Math. Anal. **38**(3), 782-794 (2006)

[36] Isett, P.: Hölder continuous Euler flows in three dimensions with compact support in time. Preprint, 2012. arXiv:1211.4065

[37] Isett, P. and Oh, S.-J.: On nonperiodic Euler flows with Hölder regularity. Arch. Rat. Mech. Anal., **221**, 725-804 (2016)

[38] Kimura, Y.: Similarity solution of two-dimensional point vortices. J. Phys. Soc. Japan., **56**, 2024-2030 (1987)

[39] Kraichnan, R. H.: Inertial ranges in two-dimensional turbulence. Phys. Fluids, **10**, 1417-1423 (1967)

[40] Krasny, R.: A study of singularity formation in a vortex sheet by the point-vortex approximation. J. Fluid Mech., **167**, 65-93 (1986)

[41] Krasny, R.: Desingularization of periodic vortex sheet roll-up. J. Comput. Phys. **65**, 292-313 (1986)

[42] Krasny, R: Vortex sheet computations: roll-up, wakes. separation. Lect. Appl. Math., AMS, **28**, 385-402 (1986)

[43] Kolmogorov, A. N.: The local structure of turbulence in incompressible viscous fluid for very large Reynolds number. Dokl. Akad. Nauk SSSR **30**, 301-305 (1941).

[44] Leith, C. E.: Diffusion approximation for two-dimensional turbulence. Phys. Fluids, **11**, 671-673 (1968)

[45] Leonard, A.: Vortex methods for flow simulation. J. Comput. Phys. **37**, 289-335 (1980)

[46] Liu, J. G. and Xin, Z.: Convergence of vortex methods for weak solutions to the 2-D Euler equations with vortex sheet data. Comm. Pure Appl. Math. **48**, 611-628 (1995)

[47] Lunasin, E., Kurien, S., Taylor, M. A. and Titi, E. S.: A study of the Navier-Stokes-α model for two-dimensional turbulence. J. Turbulence., **8**, 1-21 (2007)

[48] Majda, A. J.: Remarks on weak solutions for vortex sheets with a distinguished sign. Indiana Univ. Math. J., **42**, 921-939 (1993)

[49] Marchioro, C. and Pulvirenti, M.: Mathematical theory of incompressible nonviscous fluids. Applied Mathematical Sciences, **96**, Springer, New York (1994)

[50] Marsden, J. E. and Shkoller, S.: The anisotropic Lagrangian averaged Euler and Navier-Stokes equations. Arch. Rat. Mech. Anal., **166**, 27-46 (2003)

[51] Mohseni, K., Kosović, B., Shkoller, S. and Marsden, J. E.: Numerical simulations of the Lagrangian averaged Navier-Stokes equations for homogeneous isotropic turbulence. Phys. Fluids **15**(2), 524-544 (2003)

[52] Moore, D. W.: The spontaneous appearance of a singularity in the shape of an evolving vortex sheet. Proc. R. Soc. Lond. A **365**, 105-119 (1979)

[53] Newton, P. K.: The N-Vortex Problem, Analytical Techniques. Springer, (2001)

[54] Novikov, E. A.: Dynamics and statistic of a system of vortices. Sov. Phys. JETP., **41**, 937-943 (1976)

[55] Oliver, M. and Shkoller, S.: The vortex blob method as a second-grade non-Newtonian fluid. Comm. Part. Diff. Equ., **26**, 295-314 (2001)

[56] Onsager, L.: Statistical hydrodynamics. Nouvo Cimento Suppl. **6**, 287-297 (1949)

[57] Sakajo, T.: Interactions of two vortex sheets. Adv. Math. Sci. Appl., **8**, 631-662 (1998)

[58] Sakajo, T.: Instantaneous energy and enstrophy variations in Euler-alpha point vortices via triple collapse. J. Fluid Mech., **702**, 188-214 (2012)

[59] Scheffer, V.: An inviscid flow with compact support in space-time. J. Geom. Anal. **3**, 343-401 (1993)

[60] Shnirelman, A.: On the nonuniqueness of weak solution of the Euler equation. Comm. Pure Appl. Math. **50**, 1261-1286 (1997)

[61] Shnirelman, A.: Weak solutions with decreasing energy of incompressible Euler equations. Comm. Math. Phys. **210**, 541-603 (2000)

[62] Shvydkoy, R.:Lectures on the Onsager conjecture. Discr. Conti. Dyn. Syst. Ser.S **3**(3), 473-496 (2010)

[63] Yudovich, V. I.: Nonstationary motion of an ideal incompressible liquid. USSR Comp. Math. Phys., **3**, 1407-1456 (1963)

Research Institute for Electronic Science
Hokkaido University
Kita 12 Nishi 7, Kita-ku, Sapporo, Hokkaido
JAPAN E-mail address: gotoda@es.hokudai.ac.jp